CHEMICAL PHYSICS

Ultrafast charge transfer coupled to quantum proton motion at molecule/metal oxide interface

Weibin Chu[1,2,3], Shijing Tan[1], Qijing Zheng[1], Wei Fang[4,5,6], Yexin Feng[7], Oleg V. Prezhdo[2], Bing Wang[1], Xin-Zheng Li[8,9]*, Jin Zhao[1,10]*

Understanding how the nuclear quantum effects (NQEs) in the hydrogen bond (H-bond) network influence the photoexcited charge transfer at semiconductor/molecule interface is a challenging problem. By combining two kinds of emerging molecular dynamics methods at the ab initio level, the path integral–based molecular dynamics and time-dependent nonadiabatic molecular dynamics, and choosing CH_3OH/TiO_2 as a prototypical system to study, we find that the quantum proton motion in the H-bond network is strongly coupled with the ultrafast photoexcited charge dynamics at the interface. The hole trapping ability of the adsorbed methanol molecule is notably enhanced by the NQEs, and thus, it behaves as a hole scavenger on titanium dioxide. The critical role of the H-bond network is confirmed by in situ scanning tunneling microscope measurements with ultraviolet light illumination. It is concluded the quantum proton motion in the H-bond network plays a critical role in influencing the energy conversion efficiency based on photoexcitation.

INTRODUCTION

The semiconductor/molecule interface is one of the most important prototypical systems for different photo-energy conversion applications, including photocatalysis and photovoltaics. The photoexcitation-induced charge transfer dynamics at the interface plays a central role in a variety of energy transduction processes. In photocatalysis, an electron-hole pair is generated in the semiconductor upon photoexcitation. After that, the photocatalytic reaction is driven by interfacial charge transfer between the semiconductor substrate and the molecular media, in competition with other carrier processes, such as hot carrier relaxation, diffusion, trapping by defects, and electron-hole recombination (*1*). In photovoltaics, the molecular solar efficiency is also governed by charge transfer dynamics between the semiconductor and the molecule (*1*). Therefore, understanding the interfacial charge transfer dynamics at the semiconductor/molecule interface is essential for the sustainable development of clean energy.

At many semiconductor/molecule interfaces, the hydrogen bond (H-bond) network is naturally formed. It is well known that the H-bond network in aqueous systems plays a crucial role in the collective dynamics of charge and proton transfer (*2*–*7*). At semiconductor/molecule interfaces, the case becomes more complicated. The structure of the H-bond network is influenced by the solid surface (*8*, *9*). The existence of inhomogeneous adsorption sites, such as metal cations, oxygen anions, and defects, makes the nature of the molecule-semiconductor interaction a problem of great complexity (*10*–*12*). The interfacial charge transfer is often coupled with motions of H nuclei (protons) (*1*, *9*). Because of the light mass of H, the nuclear quantum effects (NQEs) can play an important role in H-bonded systems, such as water and interfacial water (*13*–*15*) and molecular crystals (*16*), affecting the structure and strength of H-bonds (*17*, *18*). Moreover, the dynamics of the H-bond network is also notably affected by NQEs, which mainly arise from quantum tunneling and zero-point motion of protons (*2*). The photoexcited charge transfer dynamics at the semiconductor/molecule interface involves coherent motions of charges and protons, in which the H-bond network and the NQEs come into play collectively. Studying the coherent photoexcited charge and quantum proton dynamics raises severe challenges due to the complexity, and the impact of quantum proton motion in the H-bond network on the photoexcited charge transfer dynamics at the semiconductor/molecule interface is still unknown.

The development of mixed classical-quantum ab initio nonadiabatic molecular dynamics (NAMD) makes it possible to investigate the photoexcited charge transfer at the solid/molecule interface, in which the electrons are treated quantum mechanically, yet the nuclei are classical point-like particles (*19*–*22*). Methods stemming from Feynman's path integral representation of quantum mechanics made the simulation of NQEs in large condensed phase systems feasible. The Feynman representation provides an alternative to the wave function representation of Schrödinger. It involves summation over classical-like paths, creating a classical mechanical analogy for quantum mechanics. A number of reviews have provided detailed accounts of the path integral theory, the derived methods, and a variety of applications (*2*, *23*). By incorporating quantum mechanics into molecular dynamics simulations using Feynman's path integral, one can treat the nuclei quantum mechanically by mapping each quantum nucleus onto a classical ring polymer of N replicas of the classical nuclei, with adjacent replicas connected by harmonic potentials (*23*). Ab initio path integral molecular dynamics (PIMD) is one example, which is well defined for the simulation of statistical properties. When kinetic properties are of interest, there are also

[1]Department of Physics, University of Science and Technology of China, Hefei, Anhui 230026, People's Republic of China. [2]Departments of Chemistry, and Physics and Astronomy, University of Southern California, Los Angeles, CA 90089, USA. [3]Key Laboratory of Computational Physical Sciences (Ministry of Education), Institute of Computational Physical Sciences, Fudan University, Shanghai 200433, People's Republic of China. [4]State Key Laboratory of Molecular Reaction Dynamics and Center for Theoretical Computational Chemistry, Dalian Institute of Chemical Physics, Chinese Academy of Sciences, Dalian 116023, People's Republic of China. [5]Department of Chemistry, Fudan University, Shanghai 200438, People's Republic of China. [6]Laboratory of Physical Chemistry, ETH Zurich, CH-8093 Zürich, Switzerland. [7]School of Physics and Electronics, Hunan University, Changsha 410082, People's Republic of China. [8]Interdisciplinary Institute of Light-Element Quantum Materials, Research Center for Light-Element Advanced Materials, State Key Laboratory for Artificial Microstructure and Mesoscopic Physics, Frontier Science Center for Nano-optoelectronics and School of Physics, Peking University, Beijing 100871, People's Republic of China. [9]Peking University Yangtze Delta Institute of Optoelectronics, Nantong, Jiangsu 226010, People's Republic of China. [10]Hefei National Laboratory, Hefei 230088, People's Republic of China. *Corresponding author. Email: xzli@pku.edu.cn (X.-Z.L.); zhaojin@ustc.edu.cn (J.Z.)

several other practical schemes, such as centroid molecular dynamics (*24*) and ring polymer molecular dynamics (RPMD) (*25*), applicable to large condensed matter systems. Using a combination of such path integral–based methods and NAMD, one can investigate how the quantum proton motion in the H-bond network affects the photoexcited charge transfer dynamics at the semiconductor/molecule interface at the ab initio level.

In this work, we use such a scheme to study how the NQEs and the H-bond network affect the photoexcited charge transfer at the CH_3OH/TiO_2 interface. The interface is chosen as a prototypical system for the following reasons. TiO_2 has important applications in photocatalysis and photovoltaics. CH_3OH is known as a hole scavenger on the TiO_2 surface, since it can trap photogenerated holes and prevent electron-hole recombination (*11*, *26*–*28*). Furthermore, CH_3OH can form a H-bond network on the TiO_2 surface, where H-bonds can be formed both between the adjacent molecules and at the molecule-solid interface. Previous experiments suggested that the H-bond formation may affect the photochemical reactivity (*29*). Last, the energy barrier of proton transfer in the H-bond network is comparable to the zero-point energy of the OH stretching mode, and therefore, the NQEs, including proton tunneling and delocalization, can play a critical role. All these reasons make the CH_3OH/TiO_2 interface an excellent prototypical system to investigate. We find that without the H-bond network formation, molecularly adsorbed CH_3OH on TiO_2 is not able to trap the photoexcited hole. However, if a H-bond network is formed, then NQEs will induce the proton delocalization between the adjacent CH_3OH molecules and assist the concerted deprotonation of CH_3OH to form CH_3O. As a result, the photoexcited hole can be trapped by CH_3O within several hundreds of femtoseconds. The critical role of the H-bond network is confirmed by in situ scanning tunneling microscope (STM) measurements with ultraviolet (UV) light illumination. Our results prove that the photoexcited carrier dynamics at the solid/molecule interface can be significantly coherent with the H-bond formation and NQEs.

RESULTS

Models of CH_3OH adsorption on rutile TiO_2(110)

A 3 × 1 surface cell is used to simulate the interface, as shown in Fig. 1 (A to D). We have investigated the molecular and dissociated mono-adsorption [labeled as M_M and D_M in Fig. 1 (A and B)] and molecular double adsorption, for which two CH_3OH molecules adsorb adjacently in one surface cell. For the M_M structure, the H atom in CH_3OH can form a H-bond with a bridging oxygen (O_b) on the rutile TiO_2(110) surface. Through the deprotonation, the D_M structure is formed, and in this case, H from CH_3OH forms a covalent bond with O_b. For molecular double adsorption, a H-bond can be formed between the two adjacent molecules, resulting in a CH_3OH dimer. Therefore, the intermolecular H-bond in the dimer and interfacial H-bond between CH_3OH and O_b constitute a H-bond network. We label the molecular double adsorption with and without H-bond network formation as M_D_H and M_D_nH, respectively, as shown in Fig. 1 (C and D). There are two interfacial H-bonds between CH_3OH and TiO_2 in M_D_nH, while there is one interfacial H-bond and one intermolecular H-bond in the M_D_H structure. As discussed in our previous study, the photoexcited hot hole in TiO_2 has a probability to be trapped by the highest occupied molecular orbital (HOMO) of CH_3OH if its energy is above or at least close enough to the valence band maximum (VBM) of TiO_2 (*30*). The HOMO positions based on the density functional theory (DFT) calculation of these four different structures and their abilities to trap the photoexcited hole are schematically shown in Fig. 1E. Such energy level alignments imply that only the D_M structure has the

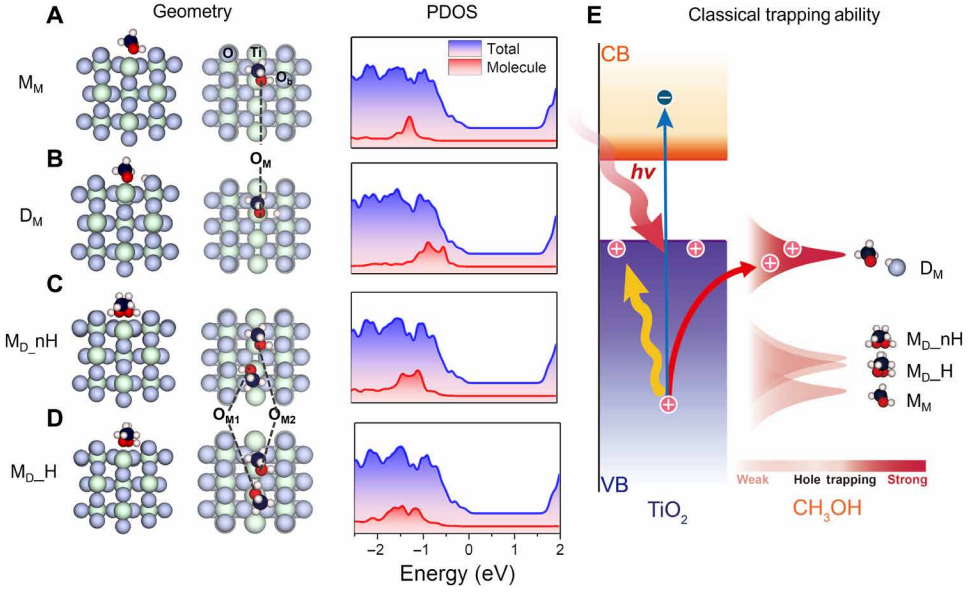

Fig. 1. Geometries and electronic structures of the CH_3OH/TiO_2 surface. (**A** to **D**) Side view, top view, and corresponding projected density of states (PDOS) for (A) mono molecular CH_3OH (M_M), (B) mono deprotonated CH_3OH (D_M), (C) double molecular CH_3OH without H-bond between molecules (M_D_nH), and (D) double molecular CH_3OH with a H-bond between molecules (M_D_H). (**E**) Schematics of the photoexcitation and hole trapping processes in CH_3OH/TiO_2. A photoexcited hot hole can be trapped by the molecule and participate in the subsequent chemical reaction. Under the classical picture, only dissociated CH_3OH, i.e., methoxy, has the ability to trap the hot hole due to the appropriate energy level alignment. CB, Conduction band; VB, Valence band.

ability to trap the hole under the classical proton picture. The HOMO of M_M has the lowest energy. The double adsorption M_D_H and M_D_nH promote the HOMO upward in energy by around 0.5 eV. Still, their HOMOs are far below the VBM of TiO_2, which makes the hole trapping unfavorable. However, the H-bond network formation at the CH_3OH/TiO_2 interface makes the proton transfer possible. The M_M and D_M structures can convert to each other by proton transfer at the interface. Similarly, the M_D_nH structure can also dissociate by transferring the proton in CH_3OH to O_b on TiO_2. Such proton transfer can tune the hole trapping ability as we discuss later.

NQEs induced proton quantum motion

To investigate the proton transfer process, we define a reaction coordinate of proton transfer as $\delta = R_{OaH} - R_{OdH}$. Here, R_{XY} is the distance between sites X and Y, where O_a, O_d, and H denote the acceptor, the donor, and the proton in the initially proton-ordered geometry. Before the proton transfer occurring, O_dH is a covalent OH bond and O_aH is a H-bond that is longer than the covalent O_dH bond. Upon the proton transfer from O_d to O_a, δ changes from positive to negative. Before considering these systems at the quantum level, it is instructive to consider the probability of proton transfer from the classical perspective. In Fig. 2, we plot the probability distributions of δ for the M_M, M_D_nH, and M_D_H systems at 100 K simulated by classical ab initio molecular dynamics (AIMD). For all the structures, δ remains positive. For the molecular adsorption structures (M_M, M_D_nH, and M_D_H), δ peaks around 0.5 to 0.7 Å, indicating that proton transfer does not occur during the simulation.

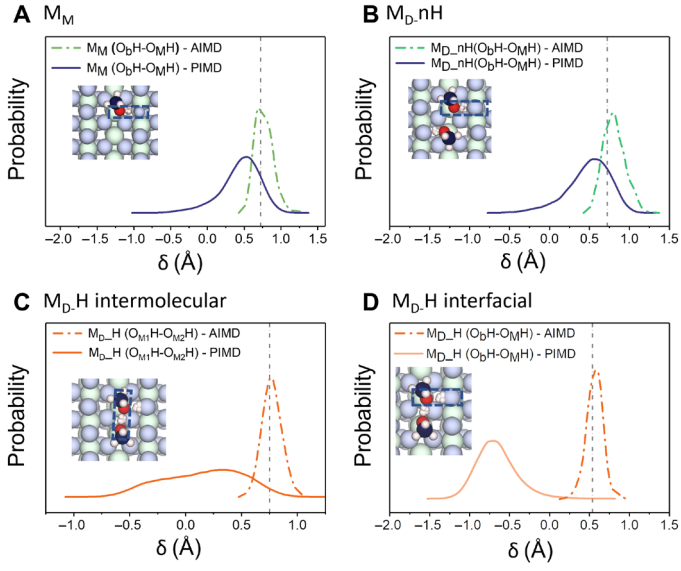

Fig. 2. Probability distributions of the reaction coordinate in classical AIMD and quantum PIMD. (**A** and **B**) Interfacial proton transfer of (A) mono molecular CH_3OH and (B) double molecular CH_3OH without the H-bond network. (**C** and **D**) The (C) intermolecular and (D) interfacial proton transfer of double molecular CH_3OH with the H-bond network. The reaction coordinate is defined as $\delta = R_{OaH} - R_{OdH}$. R_{XY} is the distance between sites X and Y, where O_a, O_d, and H denote the acceptor, the donor, and the proton in the initially proton-ordered geometry. In general, the proton transfer occurs when $\delta < 0$. The dashed lines represent results from classical AIMD simulation, while the solid lines represent results from quantum PIMD simulation. The positions of δ of the 0 K optimized geometries are indicated with the vertical dashed lines.

Now, we consider how the NQEs affect the H-bond network and proton transfer at the statistical level. This is done by comparing the probability distributions of δ obtained from the AIMD and PIMD simulations. The NQEs broaden the peak of δ and reduce the peak position to around 0.5 Å for M_M and M_D_nH, suggesting that the proton becomes more delocalized between O_b and O_M. However, there are only transient proton excursions (*31*), and no stable proton transfer is observed for these two structures. It is noteworthy that the NQEs influence the proton transfer in the M_D_H system significantly, as shown in Fig. 2 (C and D). The proton transfer coordinate δ for the intermolecular proton forms a broad distribution ranging from −1.0 to 1.2 Å, indicating that the proton becomes distinctly delocalized between the two oxygens (O_{M1} and O_{M2}). Meanwhile, the δ peak for the interfacial proton between O_b and O_{M1} changes from 0.58 to −0.73 Å, demonstrating an interfacial proton transfer process. We have verified the results with different supercell sizes and hybrid functional PBE0. More details can be found in the Supplementary Materials. Note that quantum fluctuations in H or H-bonded systems generally lead to the broadening of the position of the proton/H, which is known as the quantum delocalization effect. In the harmonic limit, quantum fluctuations can be effectively reproduced by thermal fluctuation at a higher temperature. However, for vibrational modes with different frequencies, the quantum fluctuations correspond to thermal fluctuation at different temperatures (*32*), which is different from performing a classical simulation at a higher temperature.

H-bond network makes CH_3OH a hole scavenger

The simulations demonstrate that the NQEs affect the energy level alignment at the CH_3OH/TiO_2 interface. To capture the influence of the NQEs on real-time dynamics, a practical version of the RPMD method named thermostated ring-polymer molecular dynamics is used (*33*, *34*). Figure 3 shows the time evolution of Kohn-Sham (KS) state energies in the AIMD simulation and the averaged KS energies over different beads in the RPMD simulation. The colors of the KS states show the orbital contribution by CH_3OH. In general, the NQEs lift the HOMO of CH_3OH. However, for M_M and M_D_nH, the HOMO is still below the VBM. For the M_D_H structure, in which the proton delocalization and transfer have been observed, the HOMOs of two CH_3OH are lifted above the VBM, suggesting a strong ability of hole trapping.

To confirm that the NQEs induce hole trapping, we have performed ab initio NAMD simulation based on these RPMD trajectories as shown in Fig. 4. We label these simulations as RP-NAMD. The hole is initially excited to −1.5 eV below the VBM. The NAMD simulations based on classical AIMD trajectory predict that there is a temporary hole trapping of 10 to 15% for M_M, M_D_nH, and M_D_H systems within the first 200 fs. However, afterward, the reverse hole transfer from the molecules to the TiO_2 (110) surface occurs. After reaching equilibrium, the hole trapping ability for all three systems is less than 0.1%, which is in good agreement with our previous investigations (*30*). The temporary hole trapping in the first 200 fs can be understood from the CH_3OH HOMO energy position shown in Fig. 3. In classical AIMD simulations, the HOMO of CH_3OH lies at [−1.5, −0.5] eV below the VBM of TiO_2. In our simulation, the hole is initially photoexcited to −1.5 eV below the VBM. Therefore, the temporary hole trapping can be observed in the first 200 fs. By quantum RPMD, the HOMO of CH_3OH is lifted toward the VBM for all three systems. The NQEs enhance slightly the hole trapping

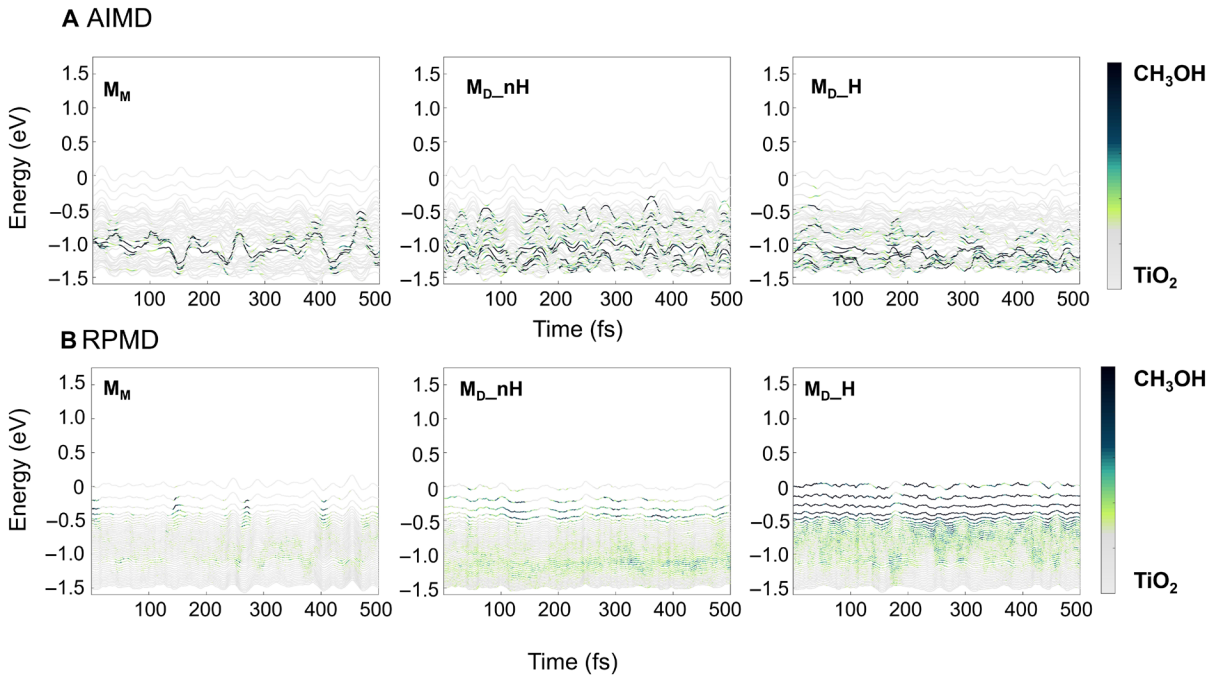

Fig. 3. Evolution of CH_3OH molecular orbitals in classical AIMD and quantum RPMD simulations. (**A** and **B**) The 500-fs evolution of KS energy levels of TiO_2 and CH_3OH in the systems with mono molecular CH_3OH, double molecular CH_3OH without the H-bond network, and double molecular CH_3OH with the H-bond network in classical AIMD simulation (A) and quantum RPMD simulation (B). The results are averaged over 32 beads in the RPMD simulation. The energy reference is set at the VBM at $t = 0$ fs. The color bar represents the contribution of CH_3OH to each KS state.

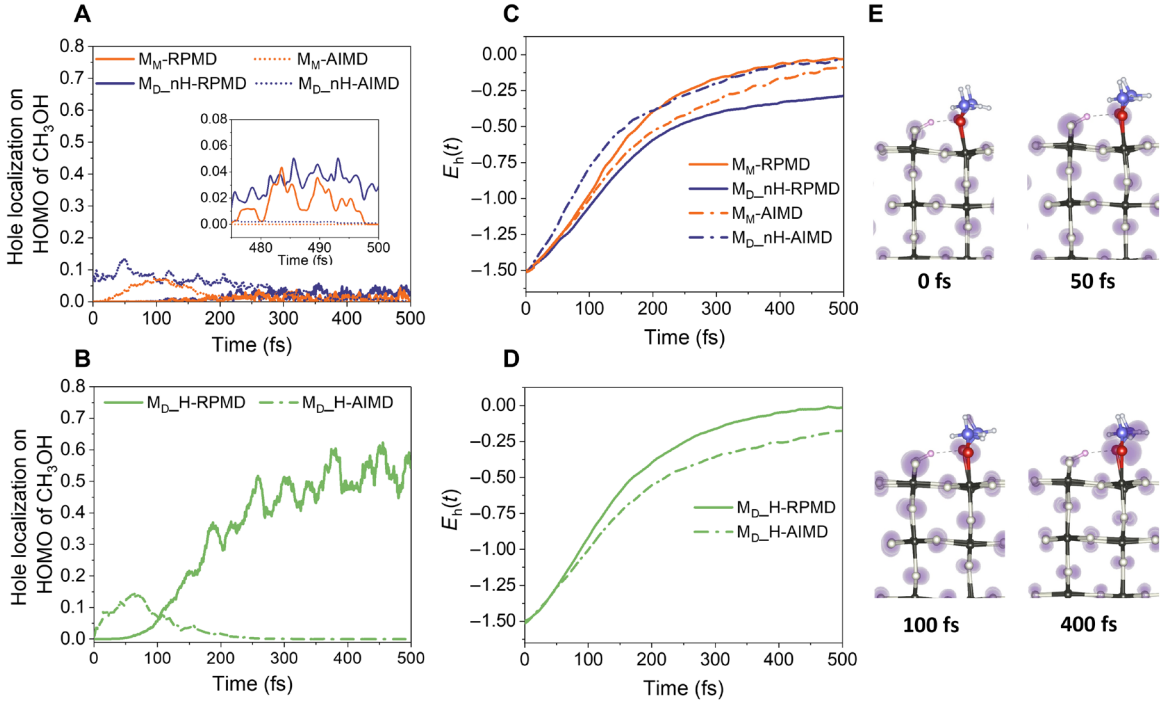

Fig. 4. Hot hole trapping and energy relaxation processes calculated with the classical AIMD and the quantum RP-NAMD. (**A** and **B**) Hot hole trapping by CH_3OH in the system (A) without the H-bond network and (B) with the H-bond network. The dynamics at the last 25 fs are shown in the inset of (A). (**C** and **D**) Hot hole energy relaxation in the system (C) without the H-bond network and (D) with the H-bond network. (**E**) Snapshots of the real-time hole density distribution in a representative trajectory of the H-bond network system. The results from the classical NAMD and the quantum RP-NAMD are indicated with dashed and solid lines, respectively.

probability in the M_M and M_D_nH structures. The HOMO of CH_3OH can trap 1 and 3% of photogenerated holes (Fig. 4A), respectively. In the M_D_H structure, the CH_3OH HOMO can trap as much as 60% of the photoexcited holes (Fig. 4B), which is comparable with the dissociated CH_3OH (*30*).

We have also checked how the NQEs affect the hot hole relaxation. For all three systems, the hot hole is initially photoexcited at −1.5 eV below the VBM [E_h (t) = −1.5 eV, t = 0 fs]. Within 500 fs, the hot hole relaxes toward the VBM. The NQEs on the hot hole relaxation in the M_M system are minor. For M_D_nH and M_D_H, NQEs have the opposite influence on the hot hole relaxation. For M_D_nH, NQEs suppress the hot hole relaxation when E_h reaches around −0.4 eV (Fig. 4C). On the contrary, NQEs accelerate the hole relaxation in M_D_H when E_h is close to the VBM (Fig. 4D). Such results can be understood from the molecular energy level localization (Fig. 3). In the AIMD simulation, the VBM and several states below it are all contributed by TiO_2 (as shown in Fig. 3A). Therefore, the hot hole relaxation in this energy range is within TiO_2. In this case, M_D_H and M_D_nH do not show a significant difference. The quantum RPMD simulation changes the molecular orbital energy distribution. As shown in Fig. 3B, for M_D_nH, the VBM is mostly contributed by TiO_2, while the VBM-1 to VBM-4 states are hybridized states contributed by the molecules and TiO_2. Therefore, in this energy region, the hot hole relaxation corresponds to the charge transfer dynamics at the CH_3OH/TiO_2 interface. By contrast, in the M_D_H system, the VBM to VBM-4 are all contributed by the molecules. Thus, in this system, the hot hole relaxation in this energy region corresponds to the intramolecular charge relaxation, which is faster than the interfacial charge transfer, since the orbital overlap is larger.

Note that the length of the trajectory used in this work is 500 fs. From Fig. 4, one can see that the hole trapping process and hot hole relaxation converge at 500 fs. Therefore, we propose that the current trajectory is able to capture the major physics. Longer trajectories can provide better sampling. It will be possible to investigate longer trajectories in the future by combining PIMD with machine learning techniques. In addition, note that in this work, we do not encounter the inverted Marcus region or a large energy bandgap, for which the standard fewest switches surface hopping needs additional corrections (*35*, *36*). Therefore, we use the standard method.

Collective quantum motion–coupled charge transfer

It is noted that the NQEs are not distinct for M_M and M_D_nH, but for M_D_H, they play a crucial role in enhancing the hole trapping, implying the critical role of the H-bond network formation at the CH_3OH/TiO_2 interface. To understand more clearly how the H-bond network correlates with the NQEs, in Fig. 5A, we analyze the statistical structural properties in the PIMD simulation. The interfacial and intermolecular δ values at each simulation step in the M_D_H structure are plotted. Note that the PIGLET thermostat is used in the PIMD simulations. The step number presented in Fig. 5 does not reflect the exact timescale. However, the simulation shows that the intermolecular and interfacial δ values are strongly correlated and evolve synchronously. Before equilibrium, these two processes happen concertedly. Namely, the proton transfer from one CH_3OH (labeled as M2 in Fig. 5B) to O_b is accompanied by the proton transfer from the other CH_3OH (labeled as M1 in Fig. 5B) to M2. After the initial proton transfer, the intermolecule δ oscillates between −0.6 and 0.7 Å, corresponding to the proton moving back and forth between the two CH_3OH molecules. The interfacial δ remains negative, indicating that the proton is always closer to O_b after the initial proton transfer. However, it oscillates coherently with the intermolecule δ, implying the collective quantum motion of the two protons.

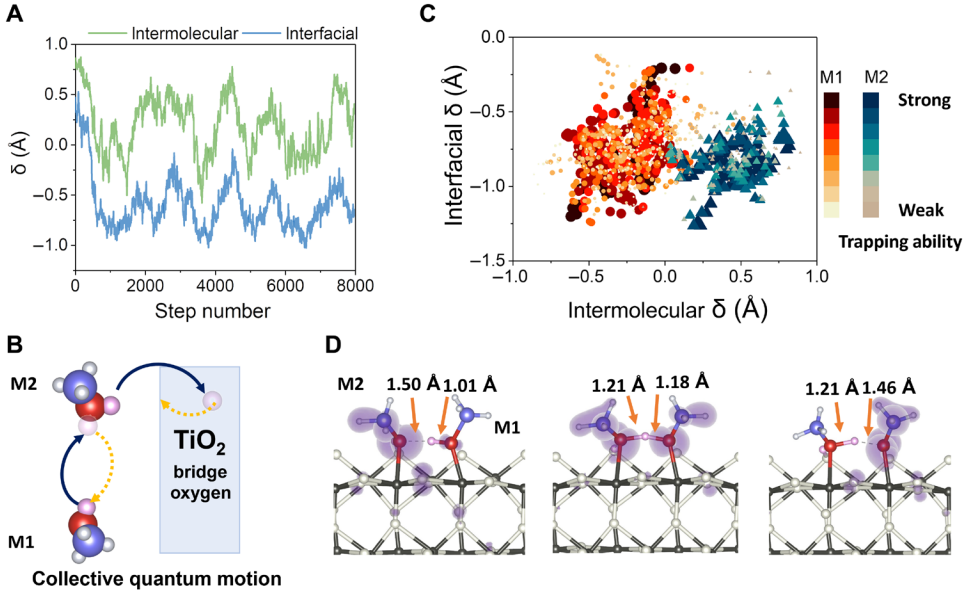

Fig. 5. Collective quantum motion and coupled hole transfer. (**A**) Evolution of the centroid of the reaction coordinate in the first 4-ps PIMD simulation. The centroid of the reaction coordinate is calculated by the average of $\delta = R_{O_aH} - R_{O_dH}$ over all the beads. (**B**) Schematic of the collective quantum motion shown in (A). The intermolecular and interfacial proton transfers occur within the equilibration collectively. (**C**) Quantum motion–coupled hole transfer between two molecules. The snapshots along the trajectory of a single bead in the RPMD simulation are used for the statistic. Both dot size and the color bar represent the hole trapping ability, which is characterized by the orbital projection of the frontier orbital on CH_3OH. The larger contribution to the frontier orbital corresponds to a stronger hole trapping ability. (**D**) Frontier hole orbital distribution in the H-bond network system of three representative geometries with $\delta > 0$, $\delta \approx 0$, and $\delta < 0$.

Therefore, we conclude that the intermolecular and interfacial quantum motions are concerted. The situation is different from the conventional stepwise proton transfer.

Such collective quantum motion of the protons is strongly coupled with the photoexcited charge transfer dynamics at the CH_3OH/TiO_2 interface. In Fig. 5C, we plot the correlation of δ with the hole trapping ability of M1 and M2. The hole trapping ability characterizes the projection of the frontier orbital on the CH_3OH molecule. The larger orbital projection on CH_3OH suggests the stronger hole trapping ability. Note that M1 and M2 can only trap the hole simultaneously when intermolecular δ is close to 0. When the proton transfers back and forth between M1 and M2, M1 is able to trap the photoexcited holes if the intermolecular δ is negative, implying that the proton transfers to M2. M2 can trap the holes when the intermolecular δ is positive, corresponding to the proton transfer back to M1. Such coupling of the charge transfer process to the quantum proton delocalization is shown schematically in Fig. 5D.

Verification of H-bond influence on photochemical reactivity by in situ STM measurements

The NQEs have been known to play a critical role in different systems from biochemistry to condensed matter (*2*, *37*–*40*). The rutile $TiO_2(110)$ surface provides an excellent prototypical templet for the NQEs. It is well known in photocatalysis and photovoltaics, and H-bond network formation, various proton transfer events, and proton-coupled charge transfer at the surface have been intensively studied (*8*, *9*, *29*, *41*–*45*). Some of the previous experimental studies suggest the existence of the NQEs at this surface. For example, H_2O on $TiO_2(110)$ was reported to be "pseudo-dissociated" (*43*). A recent high-resolution STM measurement presented a "fuzzy" feature of H_2O on TiO_2, corresponding to the frequent proton switches between the H_2O molecule and the O_b atom, analogous to the proton delocalization picture (*46*).

To further confirm the critical role played by the H-bond network, we conducted an in situ STM study by illuminating the CH_3OH molecules with UV light at 80 K. Figure 6 (A and B) shows the same area STM images before and after CH_3OH dosing to the reduced $TiO_2(110)$ surface. The bright spots represent the individually adsorbed CH_3OH monomer and dimer at Ti_{5c} sites, as can be more clearly distinguished in the enlarged images in the right. We propose that an intermolecular H-bond is formed in the CH_3OH dimer. It is known that the adsorbed CH_3OH molecules are quite stable at 80 K (*45*), unless the system is exposed to UV light (*29*, *47*) or oxygen (*48*, *49*). The photogenerated holes can be excited by UV light, which could further induce breaking of the O─H bond in CH_3OH. After 15 min of UV light illumination (Fig. 6C), some of the CH_3OH monomers have changed to exhibit an expanded feature (green arrows), while some of the dimers have changed to a much brighter round spot (red arrow). Such structural changes can be determined from the corresponding line profiles. According to the previous studies, the former feature represents the dissociated CH_3O and OH pair (*29*, *45*), and the latter one is likely a methyl formate product (*50*, *51*), generated by hole photooxidation of the CH_3OH monomer and dimer, respectively. Statistically, the reaction fraction of the dimer is 78.4% after 15 min of light illumination, much higher than that of the monomer. These experimental findings verify our conclusion that the intermolecular H-bond plays a critical role in the photochemical reaction driven by the photoexcited hole.

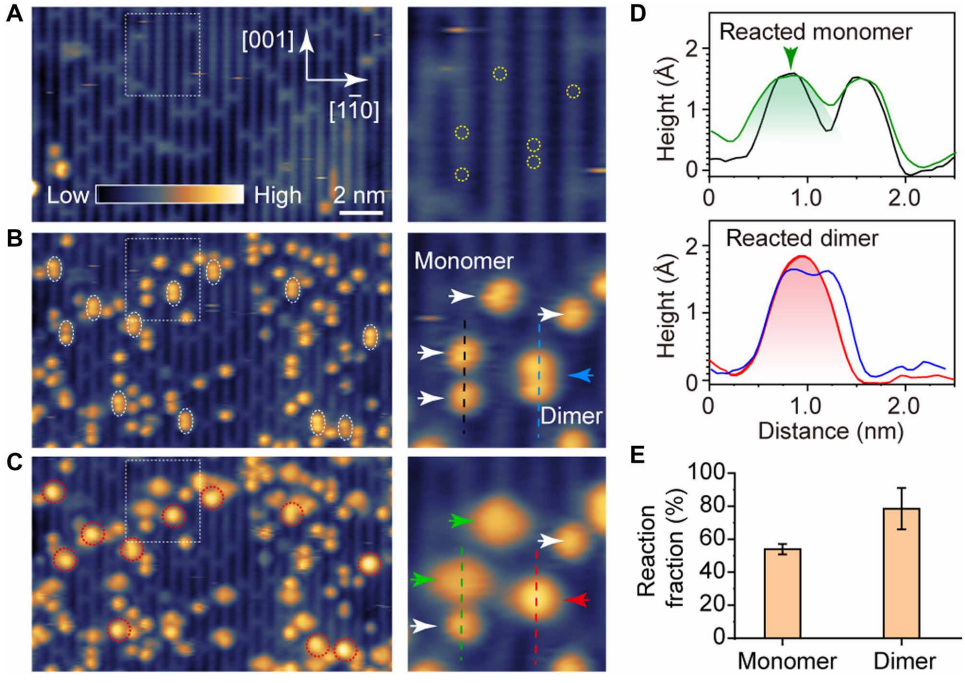

Fig. 6. In situ STM study by illuminating CH_3OH molecules with UV light. (**A**) STM image of a reduced $TiO_2(110)$ surface. (**B**) The same area image after 0.06 ml of methanol adsorption. The dashed ellipses indicate methanol dimers. (**C**) The same area image obtained after 266 nm of light illumination for 15 min. The red circles indicate the reacted dimers. The right are the enlarged areas marked by the dashed rectangles in (A) to (C). White arrows, methanol monomers; blue arrow, methanol dimer; green arrows, reacted monomers; red arrow, reacted dimer. All images are obtained at 1.0 V, 10 pA, and 80 K. (**D**) Line profiles obtained along the specific lines in the enlarged images, distinguished by the color. (**E**) The statistic fractions of reacted monomers and dimers, after 15 min of light illumination.

DISCUSSION

Note that the CH_3OH/TiO_2 system studied by both the RP-NAMD simulations and the in situ STM measurements is a simplified model system in which CH_3OH/TiO_2 is placed in a vacuum, and the coverage of CH_3OH is smaller than 1 monolayer. In the real system, there can be multilayer CH_3OH adsorption, and the other small molecules such as H_2O and O_2 may also adsorb on the TiO_2 surface. Therefore, a more complex H-bond network can be formed. We propose that the major character of proton transfer at CH_3OH/TiO_2 interface is captured by the current study. However, there is a chance to observe more abundant intermolecular proton transfer events and NQE effects with multilayer CH_3OH adsorption, which will further influence the charge transfer dynamics at the interface. That will be an interesting project for future investigation using the RP-NAMD approach.

Moreover, under the classical path approximation (CPA) (*52*), both the AIMD and RPMD trajectories are obtained on their ground state. The excitonic relaxation effects are not included. CPA was proposed to be sufficient in many solid systems because (i) a single electron excitation in a solid system creates only a small perturbation to the total electron density summed over all electrons, which is completely different with small molecules. Such small perturbation is often smaller than the thermal effects induced perturbation. (ii) The results of NAMD simulation are averaged over many trajectories and initial structures. Such averaging tends to cancel out random errors that may be encountered in individual simulated trajectories (*53*). However, the excitonic relaxation effects may still play a role in the photocatalytic process. The recently developed GW + real-time BSE − NAMD approach (*54*) provides a chance to improve CPA, and it will be interesting to understand how the excitonic effects and the NQEs come into play in the photocatalytic process in the future.

To conclude, combining the ab initio RPMD and NAMD simulation, we study how the NQEs affect the photoexcited charge transfer at the semiconductor/molecule interface. Taking the rutile TiO_2(110) surface as a prototypical system, we find that the NQEs induce the proton excursion, delocalization, and transfer at the CH_3OH/TiO_2 interface, notably enhancing the hole trapping ability. With the assistance of the H-bond network, proton transfer prohibited by classical theory will occur and make the molecule a hole scavenger. Our results successfully explain the reason why CH_3OH has been widely recognized as a hole scavenger, although the molecular CH_3OH HOMO is below the VBM by almost 1 eV (*11*, *26*–*28*). Moreover, the photoexcited charge transfer is strongly coupled with the collective quantum motion of interfacial and intermolecular protons. The finding implies that the NQEs may notably enhance the efficiency of solar energy conversion in photocatalysis, photovoltaics, and photosynthesis, in which the H-bond network formation is essential. Furthermore, we propose that such a hypothesis is not restricted to the studied TiO_2 surface and can be extended to other oxide surfaces as well.

MATERIALS AND METHODS

Modeling of CH_3OH/TiO_2 system

A 3 × 1 supercell with five layers of rutile TiO_2(110) is used to describe the CH_3OH/TiO_2 system. The bottom layer Ti and O dangling bonds are saturated with pseudo-hydrogens with nuclear charges of +1.33 and +0.66. The modeling details are in line with our previous investigations (*30*), except we use a larger supercell in this study. More discussion and verification regarding the size of the simulation cell are provided in the Supplementary Materials.

DFT calculations

The ab initio DFT calculations are carried out using Vienna ab initio simulation package (VASP) (*55*). The generalized gradient approximation functional of PBE (*56*) and the projector augmented wave (*57*) approximation for the core electrons are used. A 550-eV cutoff of planewave basis set is used for all calculations. A Monkhorst-Pack grid of (3 × 4 × 1) is used in optimization and static calculation, while a single Γ point is used in PIMD, RPMD, and RP-NAMD simulations. A good description of the electronic structure of the system and NQEs is obtained by sampling the Brillouin zone only at the Γ point [(*30*) and fig. S1], and using the Γ point only is appropriate for the description of an isolated adsorbate. The van der Waals (vdW) interactions are considered using DFT-D3 (*58*). We further evaluate vdW interaction influence on the PIMD simulation using the optB86b functional (fig. S2).

MD simulations

The classical MD simulations are performed using VASP, while the PIMD simulations are carried out using a combination of VASP and i-PI simulation software (*55*, *59*). Unless otherwise specified, all simulations use a time step of 0.5 fs at 100 K. In classical MD simulations, a 12-ps trajectory is generated using the velocity rescaling method, with the first 2 ps discarded for equilibration. In PIMD simulations, an approximate 9-ps trajectory is generated using the PIGLET thermostat to accelerate convergence with respect to the number of beads (*32*, *60*), with the first 2 ps discarded for equilibration. The parameters of the colored noise in the PIGLET algorithm are downloaded from the online repository GLE4MD. Twelve replicas are used in these PIGLET simulations. To verify the quantitative accuracy of the PIGLET simulations with 12 replicas, we further perform a PIMD simulation using local PILE thermostat with 64 replicas (fig. S3) (*61*). The influence of both vdW correction and *k*-point sampling on the PIGLET simulations is evaluated (figs. S1 and S2).

NAMD simulations

Both classical NAMD and RP-NAMD simulations are carried out using Hefei-NAMD (*62*). The NAMD simulation is based on single-particle time-dependent KS equation combining with the surface hopping scheme. CPA is applied in which the electron/hole dynamics are calculated on the basis of the predetermined trajectories using AIMD or RPMD. The classical NAMD simulations are performed with AIMD trajectories, while RP-NAMD simulations are performed in combination with thermostated RPMD trajectories. The generalized Langevin equation thermostats are used (*33*, *34*). These RPMD simulations start from several equilibrated geometries from the PIMD simulations, and 32 replicas are used. Electronic nonadiabatic transitions are propagated using the fewest switches surface hopping method with RPMD, as proposed in (*19*, *63*). Note that nonadiabatic couplings are sensitive to the position of nuclei, and the simple bead average of them does not provide physical answers, as discussed in (*64*). Therefore, we used the centroid of nuclei to calculate nonadiabatic coupling, while other electronic properties, e.g., KS energy and hole trapping ability, are still sampled with bead replicas. More method details are provided in the Supplementary Materials. For both classical NAMD and RP-NAMD, we sample 1×10^4 realizations for

500 fs with a time step of 0.5 fs. The NAMD results are based on averaging over 100 different initial configurations. The nonadiabatic couplings are calculated using CAnac with phase correction and state tracking (*65*, *66*).

In situ STM study

The experiments were conducted in a UHV STM (Omicron, LT-STM). The reduced TiO_2(110) sample (Princeton Scientific Co.) was cleaned by more than 30 cycles of sputtering and annealing up to 900 K. The STM is operated at 80 K with a tungsten tip at constant current mode. Methanol (Sigma-Aldrich, 99.9% purity) was purified by repeated freeze-pump-thaw cycles to remove dissolved gases and introduced to the sample surface via a leak valve with keeping the sample at the cryogenic STM stage. The in situ light illumination was introduced from a pulsed Nd:YAG laser (Spectra-Physics Pro250; 266 nm, 10 Hz, 10 ns). During light illumination, the STM tip was retracted about 10 μm from the surface to avoid any shadowing effect.

SUPPLEMENTARY MATERIALS

Supplementary material for this article is available at https://science.org/doi/10.1126/sciadv.abo2675

REFERENCES AND NOTES

1. H. Petek, J. Zhao, Ultrafast interfacial proton-coupled electron transfer. *Chem. Rev.* **110**, 7082–7099 (2010).
2. T. E. Markland, M. Ceriotti, Nuclear quantum effects enter the mainstream. *Nat. Rev. Chemistry* **2**, 0109 (2018).
3. Y. Litman, J. O. Richardson, T. Kumagai, M. Rossi, Elucidating the nuclear quantum dynamics of intramolecular double hydrogen transfer in porphycene. *J. Am. Chem. Soc.* **141**, 2526–2534 (2019).
4. Q.-J. Ye, L. Zhuang, X.-Z. Li, Dynamic nature of high-pressure ice VII. *Phys. Rev. Lett.* **126**, 185501 (2021).
5. W. D. Guerra, E. Odella, M. Secor, J. J. Goings, M. N. Urrutia, B. L. Wadsworth, M. Gervaldo, L. E. Sereno, T. A. Moore, G. F. Moore, S. Hammes-Schiffer, A. L. Moore, Role of intact hydrogen-bond networks in multiproton-coupled electron transfer. *J. Am. Chem. Soc.* **142**, 21842–21851 (2020).
6. L. Wang, S. D. Fried, S. G. Boxer, T. E. Markland, Quantum delocalization of protons in the hydrogen-bond network of an enzyme active site. *Proc. Natl. Acad. Sci. U.S.A.* **111**, 18454–18459 (2014).
7. G. F. Von Rudorff, R. Jakobsen, K. M. Rosso, J. Blumberger, Fast Interconversion of Hydrogen Bonding at the Hematite (001)–Liquid Water Interface. *J. Phys. Chem. Lett.* **7**, 1155–1160 (2016).
8. S. Tan, H. Feng, Q. Zheng, X. Cui, J. Zhao, Y. Luo, J. Yang, B. Wang, J. G. Hou, Interfacial hydrogen-bonding dynamics in surface-facilitated dehydrogenation of water on TiO2(110). *J. Am. Chem. Soc.* **142**, 826–834 (2020).
9. B. Li, J. Zhao, K. Onda, K. D. Jordan, J. Yang, H. Petek, Ultrafast interfacial proton-coupled electron transfer. *Science* **311**, 1436–1440 (2006).
10. U. Diebold, The surface science of titanium dioxide. *Surf. Sci. Rep.* **48**, 53–229 (2003).
11. Q. Guo, C. Zhou, Z. Ma, Z. Ren, H. Fan, X. Yang, Elementary photocatalytic chemistry on TiO_2 surfaces. *Chem. Soc. Rev.* **45**, 3701–3730 (2016).
12. T. Montini, M. Melchionna, M. Monai, P. Fornasiero, Fundamentals and catalytic applications of CeO_2-based materials. *Chem. Rev.* **116**, 5987–6041 (2016).
13. M. E. Tuckerman, D. Marx, M. Parrinello, The nature and transport mechanism of hydrated hydroxide ions in aqueous solution. *Nature* **417**, 925–929 (2002).
14. S. Habershon, T. E. Markland, D. E. Manolopoulos, Competing quantum effects in the dynamics of a flexible water model. *J. Chem. Phys.* **131**, 024501 (2009).
15. M. Ceriotti, W. Fang, P. G. Kusalik, R. H. McKenzie, A. Michaelides, M. A. Morales, T. E. Markland, Nuclear quantum effects in water and aqueous systems: Experiment, theory, and current challenges. *Chem. Rev.* **116**, 7529–7550 (2016).
16. M. Rossi, P. Gasparotto, M. Ceriotti, Anharmonic and quantum fluctuations in molecular crystals: A first-principles study of the stability of paracetamol. *Phys. Rev. Lett.* **117**, 115702 (2016).
17. X. Z. Li, B. Walker, A. Michaelides, Quantum nature of the hydrogen bond. *Proc. Natl. Acad. Sci. U.S.A.* **108**, 6369–6373 (2011).
18. W. Fang, J. Chen, Y. X. Feng, X. Z. Li, A. Michaelides, The quantum nature of hydrogen. *Int. Rev. Phys. Chem.* **38**, 35–61 (2019).
19. C. F. Craig, W. R. Duncan, O. V. Prezhdo, Trajectory surface hopping in the time-dependent Kohn-Sham approach for electron-nuclear dynamics. *Phys. Rev. Lett.* **95**, 163001 (2005).
20. R. Crespo-Otero, M. Barbatti, Recent advances and perspectives on nonadiabatic mixed Quantum–Classical dynamics. *Chem. Rev.* **118**, 7026–7068 (2018).
21. S. Meng, E. Kaxiras, Real-time, local basis-set implementation of time-dependent density functional theory for excited state dynamics simulations. *J. Chem. Phys.* **129**, 054110 (2008).
22. X. Li, N. Govind, C. Isborn, A. E. Deprince, K. Lopata, Real-time time-dependent electronic structure theory. *Chem. Rev.* **120**, 9951–9993 (2020).
23. S. Habershon, D. E. Manolopoulos, T. E. Markland, T. F. Miller, Ring-polymer molecular dynamics: Quantum effects in chemical dynamics from classical trajectories in an extended phase space. *Annu. Rev. Phys. Chem.* **64**, 387–413 (2013).
24. J. Cao, G. A. Voth, The formulation of quantum statistical mechanics based on the Feynman path centroid density. IV. Algorithms for centroid molecular dynamics. *J. Chem. Phys.* **101**, 6168–6183 (1994).
25. I. R. Craig, D. E. Manolopoulos, Quantum statistics and classical mechanics: Real time correlation functions from ring polymer molecular dynamics. *J. Chem. Phys.* **121**, 3368–3373 (2004).
26. Y. Tamaki, A. Furube, M. Murai, K. Hara, R. Katoh, M. Tachiya, Direct observation of reactive trapped holes in TiO2Undergoing photocatalytic oxidation of adsorbed alcohols: Evaluation of the reaction rates and yields. *J. Am. Chem. Soc.* **128**, 416–417 (2006).
27. T. L. Thompson, J. T. Yates, Monitoring hole trapping in photoexcited TiO2(110) using a surface photoreaction. *J. Phys. Chem. B* **109**, 18230–18236 (2005).
28. M. A. Henderson, A surface science perspective on TiO2 photocatalysis. *Surf. Sci. Rep.* **66**, 185–297 (2011).
29. H. Feng, S. Tan, H. Tang, Q. Zheng, Y. Shi, X. Cui, X. Shao, A. Zhao, J. Zhao, B. Wang, Temperature- and coverage-dependent kinetics of photocatalytic reaction of methanol on TiO_2(110)-(1 × 1) Surface. *J. Phys. Chem. C* **120**, 5503–5514 (2016).
30. W. Chu, W. A. Saidi, Q. Zheng, Y. Xie, Z. Lan, O. V. Prezhdo, H. Petek, J. Zhao, Ultrafast dynamics of photongenerated holes at a CH_3OH/TiO_2 Rutile interface. *J. Am. Chem. Soc.* **138**, 13740–13749 (2016).
31. L. Wang, M. Ceriotti, T. E. Markland, Quantum fluctuations and isotope effects in ab initio descriptions of water. *J. Chem. Phys.* **141**, 104502 (2014).
32. M. Ceriotti, G. Bussi, M. Parrinello, Nuclear quantum effects in solids using a colored-noise thermostat. *Phys. Rev. Lett.* **103**, 030603 (2009).
33. M. Rossi, M. Ceriotti, D. E. Manolopoulos, How to remove the spurious resonances from ring polymer molecular dynamics. *J. Chem. Phys.* **140**, 234116 (2014).
34. M. Rossi, V. Kapil, M. Ceriotti, Fine tuning classical and quantum molecular dynamics using a generalized Langevin equation. *J. Chem. Phys.* **148**, 102301 (2018).
35. B. R. Landry, J. E. Subotnik, How to recover Marcus theory with fewest switches surface hopping: Add just a touch of decoherence. *J. Chem. Phys.* **137**, 22A513 (2012).
36. J. E. Subotnik, A. Jain, B. Landry, A. Petit, W. Ouyang, N. Bellonzi, Understanding the surface hopping view of electronic transitions and decoherence. *Annu. Rev. Phys. Chem.* **67**, 387–417 (2016).
37. F. Pavošević, T. Culpitt, S. Hammes-Schiffer, Multicomponent quantum chemistry: Integrating electronic and nuclear quantum effects via the nuclear–Electronic orbital method. *Chem. Rev.* **120**, 4222–4253 (2020).
38. S. Chmiela, H. E. Sauceda, K.-R. Müller, A. Tkatchenko, Towards exact molecular dynamics simulations with machine-learned force fields. *Nat. Commun.* **9**, 3887 (2018).
39. S. Ghosh, S. Giannini, K. Lively, J. Blumberger, Nonadiabatic dynamics with quantum nuclei: Simulating charge transfer with ring polymer surface hopping. *Faraday Discuss.* **221**, 501–525 (2020).
40. M. Chen, H. Y. Ko, R. C. Remsing, M. F. Calegari Andrade, B. Santra, Z. Sun, A. Selloni, R. Car, M. L. Klein, J. P. Perdew, X. Wu, Ab initio theory and modeling of water. *Proc. Natl. Acad. Sci. U.S.A.* **114**, 10846–10851 (2017).
41. A. Migani, L. Blancafort, Excitonic interfacial proton-coupled electron transfer mechanism in the photocatalytic oxidation of methanol to formaldehyde on TiO_2(110). *J. Am. Chem. Soc.* **138**, 16165–16173 (2016).
42. J. Chen, Y.-F. Li, P. Sit, A. Selloni, Chemical dynamics of the first proton-coupled electron transfer of water oxidation on TiO_2 anatase. *J. Am. Chem. Soc.* **135**, 18774–18777 (2013).
43. S. Wendt, J. Matthiesen, R. Schaub, E. K. Vestergaard, E. Lægsgaard, F. Besenbacher, B. Hammer, Formation and splitting of paired hydroxyl groups on reduced TiO_2(110). *Phys. Rev. Lett.* **96**, 066107 (2006).
44. Q. Guo, C. Y. Zhou, Z. B. Ma, X. M. Yang, Fundamentals of TiO_2 photocatalysis: Concepts, mechanisms, and challenges. *Adv. Mater.* **31**, e1901997 (2019).
45. S. Tan, H. Feng, Y. Ji, Q. Zheng, Y. Shi, J. Zhao, A. Zhao, J. Yang, Y. Luo, B. Wang, J. G. Hou, Visualizing elementary reactions of methanol by electrons and holes on TiO_2(110) surface. *J. Phys. Chem. C* **122**, 28805–28814 (2018).
46. B. Dereka, Q. Yu, N. H. C. Lewis, W. B. Carpenter, J. M. Bowman, A. Tokmakoff, Crossover from hydrogen to chemical bonding. *Science* **371**, 160–164 (2021).

47. C. Zhou, Z. Ren, S. Tan, Z. Ma, X. Mao, D. Dai, H. Fan, X. Yang, J. L. Rue, R. Cooper, A. M. Wodtke, Z. Wang, Z. Li, B. Wang, J. Yang, J. Hou, Site-specific photocatalytic splitting of methanol on TiO_2(110). *Chem. Sci.* **1**, 575–580 (2010).
48. M. M. Shen, M. A. Henderson, Identification of the active species in photochemical hole scavenging reactions of methanol on TiO_2. *J. Phys. Chem. Lett.* **2**, 2707–2710 (2011).
49. M. Shen, D. P. Acharya, Z. Dohnalek, M. A. Henderson, Importance of diffusion in methanol photochemistry on TiO_2(110). *J. Phys. Chem. C* **116**, 25465–25469 (2012).
50. K. R. Phillips, S. C. Jensen, M. Baron, S. C. Li, C. M. Friend, Sequential photo-oxidation of methanol to methyl formate on TiO_2(110). *J. Am. Chem. Soc.* **135**, 574–577 (2013).
51. Q. Guo, C. Xu, W. Yang, Z. Ren, Z. Ma, D. Dai, T. K. Minton, X. Yang, Methyl formate production on TiO_2(110), initiated by methanol photocatalysis at 400 nm. *J. Phys. Chem. C* **117**, 5293–5300 (2013).
52. A. V. Akimov, O. V. Prezhdo, The PYXAID Program for non-adiabatic molecular dynamics in condensed matter systems. *J. Chem. Theory Comput.* **9**, 4959–4972 (2013).
53. S. A. Fischer, B. F. Habenicht, A. B. Madrid, W. R. Duncan, O. V. Prezhdo, Regarding the validity of the time-dependent Kohn-Sham approach for electron-nuclear dynamics via trajectory surface hopping. *J. Chem. Phys.* **134**, 024102 (2011).
54. X. Jiang, Q. Zheng, Z. Lan, W. A. Saidi, X. Ren, J. Zhao, Real-time GW-BSE investigations on spin-valley exciton dynamics in monolayer transition metal dichalcogenide. *Sci. Adv.* **7**, eabf3759 (2021).
55. G. Kresse, J. Hafner, Ab initiomolecular dynamics for open-shell transition metals. *Phys. Rev. B* **48**, 13115–13118 (1993).
56. J. P. Perdew, K. Burke, M. Ernzerhof, Generalized gradient approximation made simple. *Phys. Rev. Lett.* **77**, 3865–3868 (1996).
57. P. E. Blochl, Projector augmented-wave method. *Phys. Rev. B* **50**, 17953–17979 (1994).
58. S. Grimme, J. Antony, S. Ehrlich, H. Krieg, A consistent and accurate ab initio parametrization of density functional dispersion correction (DFT-D) for the 94 elements H-Pu. *J. Chem. Phys.* **132**, 154104 (2010).
59. V. Kapil, M. Rossi, O. Marsalek, R. Petraglia, Y. Litman, T. Spura, B. Cheng, A. Cuzzocrea, R. H. Meißner, D. M. Wilkins, B. A. Helfrecht, P. Juda, S. P. Bienvenue, W. Fang, J. Kessler, I. Poltavsky, S. Vandenbrande, J. Wieme, M. Ceriotti, i-PI 2.0: A universal force engine for advanced molecular simulations. *Comput. Phys. Commun.* **236**, 214–223 (2019).
60. M. Ceriotti, D. E. Manolopoulos, Efficient first-principles calculation of the quantum kinetic energy and momentum distribution of nuclei. *Phys. Rev. Lett.* **109**, 100604 (2012).
61. M. Ceriotti, M. Parrinello, T. E. Markland, D. E. Manolopoulos, Efficient stochastic thermostatting of path integral molecular dynamics. *J. Chem. Phys.* **133**, 124104 (2010).
62. Q. Zheng, W. Chu, C. Zhao, L. Zhang, H. Guo, Y. Wang, X. Jiang, J. Zhao, Ab initio nonadiabatic molecular dynamics investigations on the excited carriers in condensed matter systems. *Wiley Interdiscip. Rev. Comput. Mol. Sci.* **9**, e1411 (2019).
63. P. Shushkov, R. Li, J. C. Tully, Ring polymer molecular dynamics with surface hopping. *J. Chem. Phys.* **137**, 22A549 (2012).
64. F. A. Shakib, P. Huo, Ring polymer surface hopping: Incorporating nuclear quantum effects into nonadiabatic molecular dynamics simulations. *J. Phys. Chem. Lett.* **8**, 3073–3080 (2017).
65. W. Chu, Q. Zheng, A. V. Akimov, J. Zhao, W. A. Saidi, O. V. Prezhdo, Accurate computation of nonadiabatic coupling with projector augmented-wave pseudopotentials. *J. Phys. Chem. Lett.* **11**, 10073–10080 (2020).
66. W. Chu, O. V. Prezhdo, Concentric approximation for fast and accurate numerical evaluation of nonadiabatic coupling with projector augmented-wave pseudopotentials. *J. Phys. Chem. Lett.* **12**, 3082–3089 (2021).

Acknowledgments: We thank C. Verdi for discussion. W.C. thanks J.Z., X.-Z.L., and O.V.P. for mentorship and H. Chen for companionship as this work was initiated in his Ph.D. study, revised during his postdoctoral research, and finalized after he started his early career. **Funding:** J.Z. acknowledges the support of Innovation Program for Quantum Science and Technology 2021ZD0303306; National Key Foundation of China, Department of Science and Technology, grant no. 2017YFA0204904; NSFC, grant nos. 11974322 and 11620101003; and the informatization plan of Chinese Academy of Sciences, grant no. CAS-WX2021SF-0105. X.-Z.L. acknowledges the support of NSFC, grant no. 11934003. O.V.P. acknowledges the support of the U.S. National Science Foundation, grant no. CHE-1900510. S.T. acknowledges the support of NSFC, grant nos. 21972129 and 11904349. The PIMD simulation was performed at the Environmental Molecular Sciences Laboratory at the PNNL, a user facility sponsored by the DOE Office of Biological and Environmental Research. The time-dependent NAMD simulation was performed at the Hefei Advanced Computing Center. **Author contributions:** J.Z. conceived the idea. W.C. developed the method and performed the simulation under the supervision of J.Z., X.-Z.L., and Q.Z. S.T. and B.W. performed the in situ STM measurements. W.F., Y.F., and O.V.P. provided helpful suggestions. W.C. and J.Z. wrote the manuscript. All authors discussed the results and commented on the manuscript. **Competing interests:** The authors declare that they have no competing interests. **Data and materials availability:** All data needed to evaluate the conclusions in the paper are present in the paper and/or the Supplementary Materials.

Submitted 24 January 2022
Accepted 3 May 2022
Published 17 June 2022
10.1126/sciadv.abo2675

ScienceAdvances

Ultrafast charge transfer coupled to quantum proton motion at molecule/metal oxide interface

Weibin ChuShijing TanQijing ZhengWei FangYexin FengOleg V. PrezhdoBing WangXin-Zheng LiJin Zhao

Sci. Adv., 8 (24), eabo2675. • DOI: 10.1126/sciadv.abo2675

Science Advances (ISSN) is published by the American Association for the Advancement of Science. 1200 New York Avenue NW, Washington, DC 20005. The title *Science Advances* is a registered trademark of AAAS.